Wildlife Telemetry Drone

WTD: Willem Arjana, Chris Gass, Stephen Kuluris, Reejay Martinez, Alex Moore, Leonard P. Peshlakai, Trevor Petersen, Lucas Philipsen, Dylan Steyer

May 1, 2015

Northern Arizona University Engineering Department

May 1, 2015

Wildlife Telemetry Drone Team
Northern Arizona University

To Dr. Michael Shafer,

We are pleased to submit this report documenting the research, analysis, and results for the drone for wildlife telemetry that we've worked on throughout this semester. We'd like to thank you for providing us with the opportunity to work on such an exciting project, and the electrical engineers in particular would like to thank you for reaching out to our EE 476C capstone class to bring us on board.

We began this project as a tool to aid in the research of bat habitats for use in the College of Forestry, Engineering and Natural Sciences at Northern Arizona University. The current methods for conducting such research are strenuous and time consuming due to the requirement of finding vantage points of high ground in order to get a clear signal from radio telemetry tags attached to the bats to triangulate their location. This projects aims to develop an autonomous drone to collect wildlife radio telemetry measurements in a more efficient manner by flying at multiple locations, expediting the data collection process. To achieve this, a quadcopter-style drone was built and outfitted with an antenna. The drone flies straight up, rotates while collecting signal data, then lands and sends the data to a separate computing device to be processed into a latitude and longitude location where the bats are likely to be found.

At this time, a functional prototype has been created which can fly vertically into the air, record telemetry data, and offload that data to an external computer for filtering and display. A manual override is in place to ensure user control at all times, and a ground station application has been created to control all basic functions of the drone. The drone is backpackable and can sustain drops of at least five feet with only field-repairable damage. We feel that these results warrant a continuation of the project, as this design has proven that it can work, but is not yet in a state that would make sense for researchers to use. The drone would benefit from a number of improvements in frame construction, wireless communication, receiver capability, and general ease of use before deployment in the field.

This report explains what was used in the drone and why it was used, while providing details of the analysis undergone, how specifications were met, an overview of the projected and final budget, and a summary of work for the future. In addition to this report, we've created an owner's manual and extensive documentation for future teams to continue work on the drone

We're proud to present the results of this project, and we look forward to seeing future developments and iterations of the wildlife telemetry drone.

Sincerely,
Wildlife Telemetry Drone Team

Table of Contents

List of Tables and Figures

Tables

Figures

1. INTRODUCTION

The Northern Arizona University Forestry Department (henceforth referred to as NAUFD) currently tracks bat colonies throughout large areas in the forests of Northern Arizona. Bats are captured at night while they are active, and a small transmitter is placed upon each of the captured bats. Field researchers can then track the transmitted signal to the location of the roosting bats during the day. In order to locate these colonies, the signal from the transmitter must be recorded at multiple sites. By noting the direction at which the signal was recorded, the location of the colony can be triangulated. However, in order to obtain a usable signal, high vantage points are required, ideally on a ridge or small mountain. The researchers must cross-country hike to reach a suitable site before recording the signal, wasting valuable time and limiting where and when the signal can be recorded. The current process allows bat colonies to be located, but there is an opportunity to improve this process.

One method for improving the current locating process is the use of an Unmanned Aerial Vehicle (UAV), otherwise known as a drone. A drone would allow for the signal from the transmitter to be recorded from more locations, as the drone could be flown vertically to a height where it can receive the signal as effectively as a researcher would on a ridge or hill. The cross-country hiking currently necessary to reach those sites could therefore be eliminated. A drone could also potentially fly to multiple locations and record the signal at each, allowing for triangulation of a colony's location without requiring the field researcher to hike extensively.

The team has been tasked with designing and building a drone that can be used to record these signals, allowing for easier tracking of the bat colonies. While initially completing only vertical flight to record signals, the drone is to be built with the intent of taking recordings at multiple points in one flight.

2. SPECIFICATIONS

Achieving reliable flight with a UAV is a complicated process, and the addition of signal acquisition adds to the complexity of the system. Due to this complexity, a large number of specifications were assigned by the client, Dr. Michael Shafer. The following list outlines the specifications needed for an initial drone to be completed.

Table 1. Project specifications.

	Specification
Flight/Telemetry	Takes off vertically and lands within 5m of the same point
	Flies a distance of 3km with telemetry equipment attached
	Accurately outputs a signal amplitude and GPS pairing according to telemetry data
Usability	Easily fits in a hiking backpack (approximately 50x30x30cm)
	No additional training required to operate
	Allows signal and direction data to be transferred to an external device
Safety	Only predictable, field-repairable damage sustained for 5ft drop
	Manual override of autonomous flight systems is available at all times
	Drone power circuit disengages after drone sustains a fall of 5ft
Liability	Complies with FCC and FAA regulations

Of these specifications, all have been fulfilled except for three. The ways in which these specifications were fulfilled will be discussed later in report. The three that were foregone are shown below.

- Flies a distance of at least three kilometers with telemetry equipment attached
- No additional training required to operate
- Drone power circuit fuse must break after drone sustains a fall of 5 ft

The first of these, 3 kilometer flight, was found to be unnecessary for the drone in its current state. For researchers, it would be ideal for the drone to take fully autonomous triangulation flights. However, FCC (Federal Communications Commission) and FAA

(Federal Aviation Administration) regulations disallow UAV flight outside of the field of vision of an operator. As a result, this specification conflicted with our requirement to adhere to these regulations, and had to be foregone as a result.

As a result of the same FCC and FAA regulations, we determined that it would not be possible to send someone into the field with this drone with no training at all. It is important that one understands these regulations, and how to manually override the drone if an issue comes up. Therefore, we've foregone this specification, but decided to include a user manual with the drone.

The last of these specifications, a battery breakaway to disconnect the battery after a fall of five feet or greater, proved to be a project in itself, that would take more time than we were willing to allot to it given our more pressing priorities with this drone. We found that no off-the-shelf designs exist for releasing a battery of the size we used upon impact, and that existing drone designs do not use such a mechanism. We also found that the most pressing concern for lithium polymer battery safety is to avoid punctures, and we've taken appropriate measures to protect the battery, which will be outlined in the mechanical design section of the report.

3. DESIGN TEAM OBJECTIVES AND DELIVERABLES

The team determined that breaking into three subgroups would be the most effective means of completing this project. The three subgroups were decided to be Mechanical, Avionics and Telemetry. The tasks and goals for each of these teams are outlined below.

3.1 Mechanical

- Create a frame capable of carrying needed payload and surviving a crash
- Design a propulsion system capable of lifting payload
- Build an antenna to telemetry team's specifications that is compatible with frame
- Design failure points to allow for field reassembly after a crash
- Ensure that final design can be disassembled to fit in a standard backpack

3.2 Avionics

- Find or create an avionics system that can fly the drone by itself
- Find or create a controller that will control all the components of the drone and find or write open-source code for that controller to connect all of the electronic systems together
- Create a manual override system using an RC controller
- Create a ground station that will receive and display info to the user that includes triangulation data and the location of the drone every x minutes through either Bluetooth or Wi-Fi
- Ensure that any electromagnetic interference (EMI) generated by the motors does not interfere with the telemetry equipment
- Wire all of the components together in a safe and compact manner

3.3 Telemetry

- Design a prototype three-element Yagi-Uda antenna, commonly known as a "Yagi antenna"
- Construct a telemetry system, including the aforementioned antenna and a receiver that can output data to the drone's on-board computer

- Ensure that antenna and receiver are not receiving extra noise and/or interference from either the motors, any avionics circuitry, or other miscellaneous electronics
- Use MATLAB to create a filtering algorithm to eliminate any remaining noise and/or interference and display the greatest amplitude paired with time and GPS heading at that time

4. INITIAL RESEARCH

Much of the work done thus far has been research. The innovative nature of the project required knowledge from many fields of study, and the sources found in this research reflect this. Presented below are selections of some sources which have proven to be of the most benefit toward the evolution of the design.

4.1 Mechanical

One source that has proven particularly useful in designing powertrain elements is *Basic Helicopter Aerodynamics, Second Edition* by J. Seddon and Simon Newman, part of the AIAA Educational Series. This book provides explanations of the fundamentals behind rotor-craft flight. The equations and explanations guided the derivations performed to gain a fundamental understanding of how the rotors produce thrust and the power required to produce it. From this it was possible to find suitable propeller dimensions for the thrust required, suitable motors to turn the propellers, which then dictated the amperage of electronic speed controllers necessary, and a suitable battery voltage.

4.2 Avionics

The majority of the concepts related to the avionics system are straightforward, but communication with the Pixhawk flight controller requires the use of a new protocol and library which has not yet been used in the way we have intended.

The first major source is the library's traditional code documentation [1]. This includes comments within its code, a web page describing the many available enumerations, and a couple of undetailed example programs. The library, it seems, was meant to provide control to humans rather than assist an autonomous search as we will do.

A second major source has been the community-edited and 3DRobotics-funded ArduPilot wiki, a wiki for the open-source flight control software at the core of the Pixhawk flight controller [2]. The wiki contains information for similar, but far from identical, processes. Should we need to modify the Pixhawk itself, this wiki will be our greatest resource.

Finally, a personal project of a published computer scientist and electrical engineer, William Premerlani, GE, known as MatrixPilot has proven to be useful [3]. It's a MAVlink-

capable autopilot comparable to the system on the Pixhawk, but MatrixPilot's GitHub repository is remarkably well documented including how an autopilot handles MAVlink from its point of view.

We've also included a source that discusses practical electromagnetic shielding, for use in the event that our motors cause interference with the telemetry equipment of the drone [4].

4.3 Telemetry

Biotelemetry is the term used to describe techniques that incorporate the instrumental gain of a transmitter and receiver to transmit information from a living organism (e.g. bats) and its surrounding environmental factors to a remote observer (e.g. NAUFD biologists). In our research, we came across a website, which is hosted by Holohil Systems Ltd., which has a plethora of information regarding this task. It has given us a greater understanding of how frequencies differ in regards to different devices and their merits. The information acquired from this site has been a major contribution to our preliminary research on efficient methods used to track bats. The site categorizes different transmitters based on current attachment method, weight (in grams), life expectancy (in weeks), and antenna type. These devices are currently used by researchers of various disciplines, such as biologists, scientific researchers, and conservationists. There is a practical description that explains in detail for our current transmitter (LB-2X) how differing temperatures can affect the transmitter based on the interval between pulses [5].

Another source of information was Dr. David Dalton, who works for Photometrics in Tucson, Arizona. He aided us in deciding what type of antenna would be best for directional tracking. He also gave us some advice regarding various methods for tracking bats [6].

We investigated various metals to suit our requirements and constraints and examined how they compared in aspects such as conductivity, density, permittivity, and permeability. It was discovered that pure aluminum (Al) provided the strongest attributes for receiving the most reliable signal, and would be lightweight and durable enough for our clients' rugged terrain [7].

5. DESIGN DECISIONS AND ANALYSIS

Over the course of this project, all three teams have worked together to decide what designs and components are best suited to create a working design that will lead to a product for the Forestry Department to use in the field. These design decisions and their justifications are shown below, divided according to subteam.

5.1 Mechanical

The mechanical team was in charge of constructing a physical system to lift the telemetry equipment for tracking flights. The deliverables for the mechanical team included a backpackable frame capable of flight, landing gear to protect components from damage upon a possible crash, and protective systems for the battery and electronics.

5.1.1 Prototype Frame

The mechanical team began by constructing a prototype frame to begin testing. Among these initial tests was a failure point test to ensure the drone only receives easily repairable damage in the event of a crash. The completed test was designed to find a fastener configuration of the arm to the baseplate that would allow failure of the fastener near 10 lbs., which is below the failure point of both the 6061 aluminum arm and the 7075 aluminum base plate. A 12-inch arm was cut from the aluminum and holes were drilled in the base plate and the arm. A bolt and nut was then used to connect the arm to the base plate. The preload of the bolt was assumed to be zero as the nut was tightened to finger tight. The arm was end loaded until failure, to simulate and end load from impact with the ground. The results of the test are shown in Table 1.

Table 2. Fastener testing results.

Bolt type	**Nut type**	**Loading at failure** (lbs)	**Failure mode**
8-24 Nylon	8-24 Nylon	2	Sheared threadings of the nut and bolt
10-32 Nylon	10-32 Nylon	3	Sheared threadings of the nut and bolt
6-24 Zinc	6-24 Zinc	No Failure	NA
6-24 Zinc	6-24 Brass	No Failure	NA
6-24 Brass	6-24 Brass	No Failure	NA
6-24 Brass	6-24 Zinc	No Failure	NA
6-24 Zinc	6-24 Nylon	9	Sheared threads in the nut
10-32 Nylon	10-32 Brass	9.5	Rupture at the head of the bolt

As a failure load of roughly 10 lbs. was desired, the combination of 10-32 nylon bolt and brass nut was chosen, being the closest to the desired value. This combination also resulted in a consistent and predictable failure mode of shearing the bolt at the head, another desired trait. A drop test was conducted, which consisted of dropping the system at multiple angles from five feet to ensure that the failure piece performs as expected. The nylon bolt was shown to shear at the head for these heights, allowing for quick reassembly of the drone with minimal damage to critical components.

5.1.2 Thrust Calculations

Another analysis task which fell under the mechanical team's skillset was selecting propellers capable of producing enough thrust to lift the system. The propellers are the driving component for the entire propulsion system design. Once propellers are selected, motors need to be selected which are capable of spinning them, and electronic speed controllers which are capable of handling the current loads of the motor. To select propellers, a code was developed

to approximate the maximum thrust a given propeller can produce, and the power required to produce that thrust. Several assumptions were made in this development, due to the lack of detailed information available for off-the-shelf parts marketed to hobbyists who may not necessarily have an engineering background.

With the thrust approximation code complete, the team assumed a total vehicle mass of approximately six pounds leading to a desired maximum thrust of about 12 pounds to maintain maximum control authority over the vehicle. There were a few possible propellers which would be suitable, including 15” x 5.5” carbon fiber propellers and 16” x 4” carbon fiber propellers. The 16” x 4” propellers were selected because their lower pitch is better suited for hover applications, and increases stability by damping out effects of small perturbations in motor speed. For further details on the analysis performed, and to view the developed code, see Appendix A.

5.1.3 Final Frame

The mechanical design team has made many improvements from the prototype when fabricating the final frame. Many design choices were made with client specifications in mind. New aspects implemented in the final frame design were detachable arms, nylon failure points at the baseplate-arm connection in both rotation and bending, a larger baseplate, a detachable electronics box, and landing gear that also allowed a connection point for the antenna. The final frame design constructed with CAD software is shown in Figure 1 below.

Figure 1. Final frame modelled in CAD.

The detachable arms use a spring-pin connection that allows the square tubing arm to slide inside a permanent square tubing attachment to the baseplate. This connection is shown in Figure 2 below.

Figure 2. Spring-pin connection for detachable arms.

The arm then snaps into the permanent square tubing on the base plate. This design was chosen for its quick release ability, which aids in meeting the specification of having a collapsible vehicle. Holes were drilled through the arms, further lightening them. This can be seen in Figure 3 below.

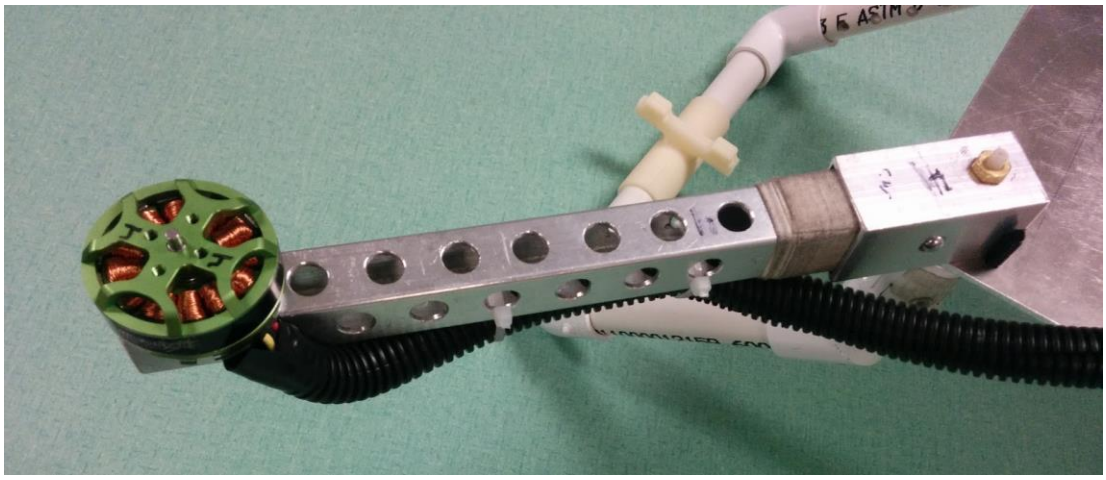

Figure 3. Arm connected to drone.

The permanent square tubing on the baseplate, used in the spring clip attachment of the arms, were connected using designed failure points. These failure points included a nylon 10-24 bolt attachment, as was determined necessary by the experiments outlined in Table 1. The nylon bolt and brass nut held the tubing from a vertical displacement, while two nylon button fasteners held the tubing from rotating. The placement of the rotation failure pieces was first tested on the prototype baseplate. Holes were drilled so that the nylon rotation prevention pieces were flush with the square tubing for one test, and with a 1/10” inlay on the square tubing piece. The 1/10” inlay gave a tighter fit to the failure pieces in preventing rotation, and therefore, were used in the final frame design. The combination of nylon connections in the vertical and horizontal planes allowed the arm to disconnect from the baseplate upon a crash, regardless of the direction of the impact. The failure of these pieces protects other, more expensive, or less field-repairable pieces. Therefore, having these pieces allows the drone to survive a 5 foot drop with only field repairable damages, as specified by the client. The operator of the drone in the field needs only to carry spare nylon bolts and button connectors in case of a crash.

The final frame design uses a larger baseplate at 11x11” so that the electronics can more easily fit on the drone. This design choice was made after realizing that the prototype baseplate of 8x8” was too small to fit an impact resistant box for the electronics. The detachable box was chosen because it met the size constraints, and could fit all electronics in it. It was chosen to have Velcro to attach the electronics box to the baseplate, because it would make the drone more collapsible, and it allows the electronics to stay completely connected with the exception of disconnecting the ESCs. This makes the drone more user friendly, because the operator does not need to reconnect any complicated electronics. One inch thick foam padding was used to pad the interior of the box, to protect all electronics housed within. A foil tape coated divider also provided two compartments that were EMI shielded to allow the receiver to be placed within its own shielded compartment. A picture of the drone displaying this box is shown in Figure 4.

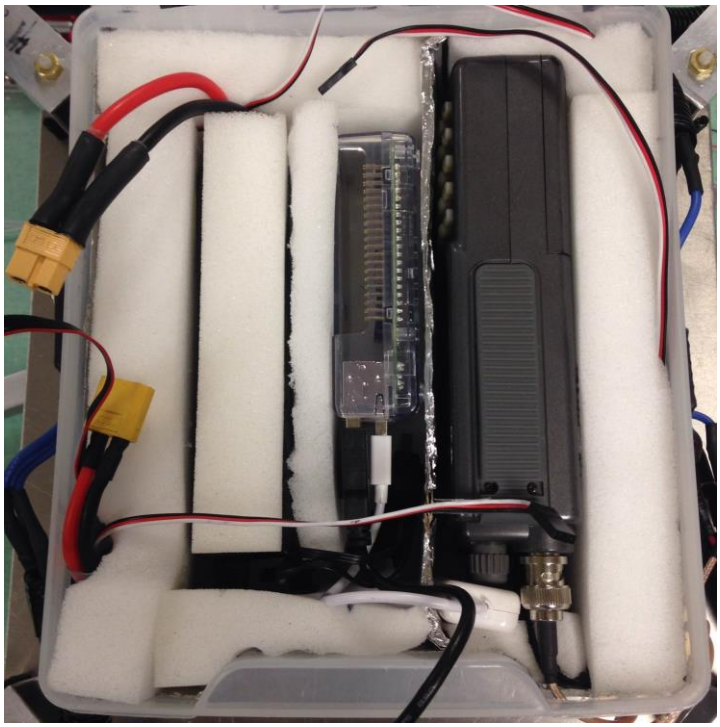

Figure 4. Box for protecting electronics and insulating receiver from EMI.

5.1.4 Landing Gear

Lastly, the mechanical team implemented landing gear that doubled as an attachment point for the antenna. The landing gear material was chosen to be PVC, so that it would have no interference with the antenna, and for its availability and cost effectiveness. The landing gear was connected through the same nylon bolt connecting the square tubing to the baseplate. This was done, so that the nylon piece would fail upon hard landing on the gear or an arm. A 45 degree attachment piece was used to offset the landing gear legs away from the frame, creating a lever arm to help break the nylon connection upon hard landing landings, absorbing a portion of the impact. The attachment point of the antenna was done through two 3D-printed pieces that attached to each leg of the landing gear and the antenna boom. The 3D-printed pieces were chosen for their customizable dimensions to fit the boom and PVC and because of the ability to make and carry extra 3D-printed parts in the field, again allowing for more field-repairable failures. The landing gear can be seen in Figure 5 below.

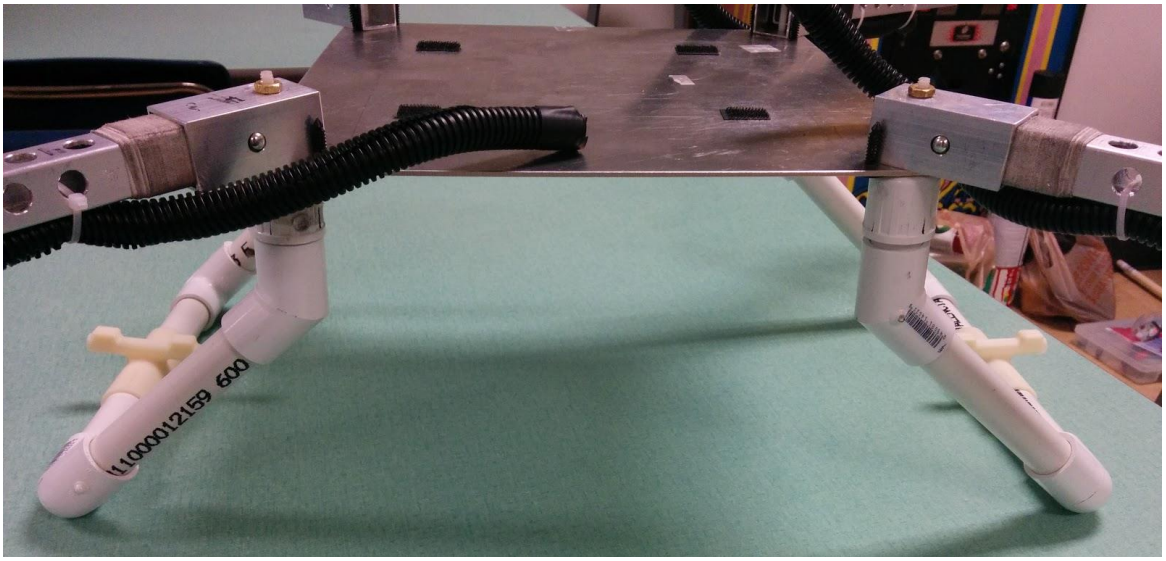

Figure 5. Landing gear attached to frame.

5.1.5 Battery Breakaway

As stated in the specifications, a battery breakaway was not implemented this semester. Current drones on the market do not feature such a device, making the design of this breakaway its own ambitious project apart from this one. Research was done into a level

actuated device, using the landing gears affixed to the arms to pull the battery connector away from the battery. However, a prototype revealed the actuation was not enough to effectively pull the connector apart. The lever design also only allowed for actuation of the battery breakaway if landing was upon the arms. Side impacts, therefore, would not disable the battery.

An inertial mass system was also considered to separate the connector. However, this method required a more easily disconnected battery connector than was currently implemented. A magnetic connector was considered, but the high current from the battery prevented current designs from being used, requiring a new magnetic system to be designed and built. This was deemed to be beyond the scope of this project, as a new connector would require extensive testing to ensure it could reliably handle the current and not disconnect unexpectedly, as this could be catastrophic during high altitude flights. The use of an inertial disconnect system in combination with a magnetic connector was considered the most viable option, with more research and development being necessary in the future to implement this idea.

To prevent fire hazards associated with the lithium polymer battery used in the drone, a plastic case was implemented to provide puncture protection, eliminating one major source of hazard to the battery. A one inch thick layer of foam also padded the battery and all other electronics in the case, preventing jostling or additional impact to the battery. A battery breakaway should be implemented before full flights in the forest, but the current safety features allow for safe test flights as development is continued.

5.2 Avionics

The avionics design considerations included three main components: the flight controller, the on-board computer, and the ground station. The flight controller, a Pixhawk, and the on-board computer, a Raspberry Pi, are in constant communication and make the entirety of the calculations in regards to flight. Additionally, their communication allows the Raspberry Pi to record data from the Pixhawk's sensors for telemetry purposes. The stripped-down system itself can be viewed in Figure 6.

Figure 6. Early prototype demonstrating Pixhawk and RPi function.

The Pixhawk is a PID control system with many standard and feedback inputs which outputs pulse widths to the speed controllers, thus maintaining flight. The Raspberry Pi sets flight paths relative to the drone's location at the time of launch, records different forms of data, communicates with the ground station, and is fully expandable.

Communication between the Pixhawk and Raspberry Pi is accomplished through a serial communication protocol known as MAVLink. MAVLink has not yet matured and is not well documented. However, some relevant information can be found in the drone's internal documentation, which should be all a developer will need to continue this project. Although the communication is currently performed through USB 2.0, UART is also a possible option through the Pi's GPIO pins and the TELEM 2 port on the Pixhawk. It's recommended that UART only be used in the case that additional USB ports are required for future purposes.

Through MAVLink, the Pi receives sensor data, sets flight paths, and performs other functions. The flight paths are calculated relative to the drone's position at launch and are sent to the Pixhawk as "mission items" using the same method as the mission planner programs. The Pixhawk, however, has a priority system in place that prefers RC controller input to serial

communication. This is important to the last component of the avionics system, the RC controller. A relatively long-range RC controller is included for manual flight but is only necessary in emergency cases and for meeting FAA requirements. Assuming no failures, it will not be used outside of manual testing, but users must be able to operate it nonetheless.

5.2.1 Pixhawk

The Pixhawk is our flight controller. In terms of processing power, it's comparable to a Raspberry Pi but runs a barebones operating system known as NuttX and whichever flight control firmware is necessary. For our purposes, it is loaded with ArduCopter, a subset of ArduPilot. The firmware is configurable through one of two available "mission planner" software packages: Mission Planner or APM Planner. We found APM Planner to be more effective for this project, as it is more straightforward to use and available for Linux and Mac OS X, whereas Mission Planner is only available for Windows. The Pixhawk and its various ports can be seen in Figure 7 below.

Figure 7. Pixhawk flight controller [8].

5.2.2 Raspberry Pi

The Raspberry Pi is a single-board computer with an ARM processor. Our Raspberry Pi is version 6, as opposed to the common version 7 found in smartphones for the previous five years. Its processor isn't especially quick but has been sufficient for this project and should continue to be in the future. Currently, three of the four USB ports are in use by the audio adapter, Wi-Fi dongle, and Pixhawk. The Raspberry Pi and its inputs can be seen in Figure 8 below.

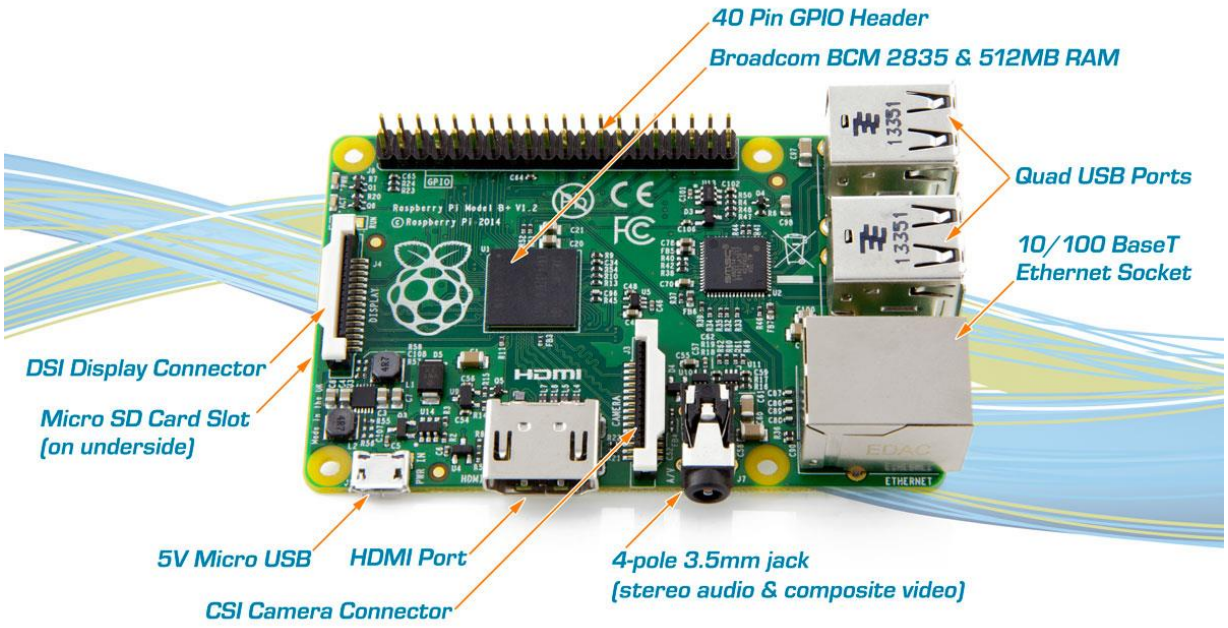

Figure 8. Raspberry Pi [9].

In terms of software, the Pi is running Raspbian, an ARMv6 version of Debian. It is configured to not use a graphical interface on boot but has OpenBox and Tint2 installed for an interface. As part of this project, we have written a program to perform tasks on the drone that is currently unnamed and has been referred to as "the program" or "custom software." It is written entirely in C and is placed in the Code directly of the home directory. A boot script in Debian's init.d configuration runs this program automatically. This program receives commands from the ground station

5.2.3 Ground Station

The ground station is an easy-to-use Android application but could take any form. Android devices, however, always have GPS devices, do not require external peripherals, and

are easily replaceable. Therefore, this is the form we chose for our ground station. With the exception of holding the safety switch on the drone itself, all control of the drone can and should be done through the ground station.

Android Studio was used in developing the ground station and is required in order to place the app onto an Android device as there are no packages (an APK file) prepared. Once finalized, a package should be made. The app is capable of running on any recent device, but the device should have a sufficient resolution. During development, a Nexus 7 with a resolution of 1080x1920 was used but the app will work on resolutions significantly lower as well. A screenshot of the ground station can be seen below.

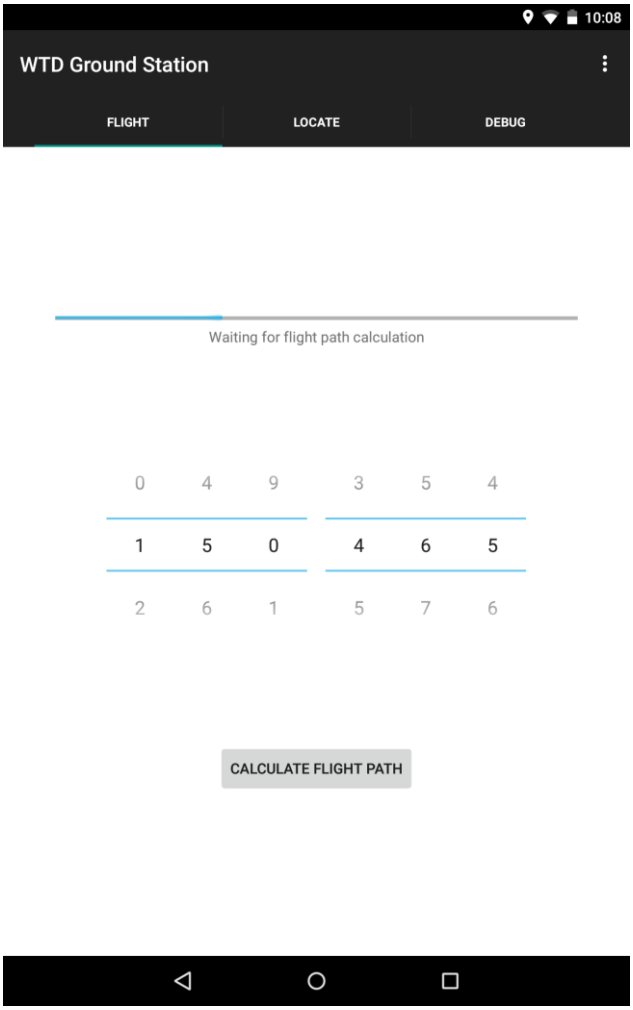

Figure 9. Screenshot of the ground station's flight screen.

The ground station contains three tabs: Flight, Locate, and Debug. The Flight tab, as shown in Figure 9, shows the progress of the flight process, frequency input, and a multi-use button used to initiate the main phases. The Locate tab, once developed, will contain a map displaying the estimated location of the tagged bat, the location of the ground station, and the heading of the ground station. The Debug tab exists for development purposes, as well as for manual control and troubleshooting. The current implementation of the debug tab is shown in Figure 10 below.

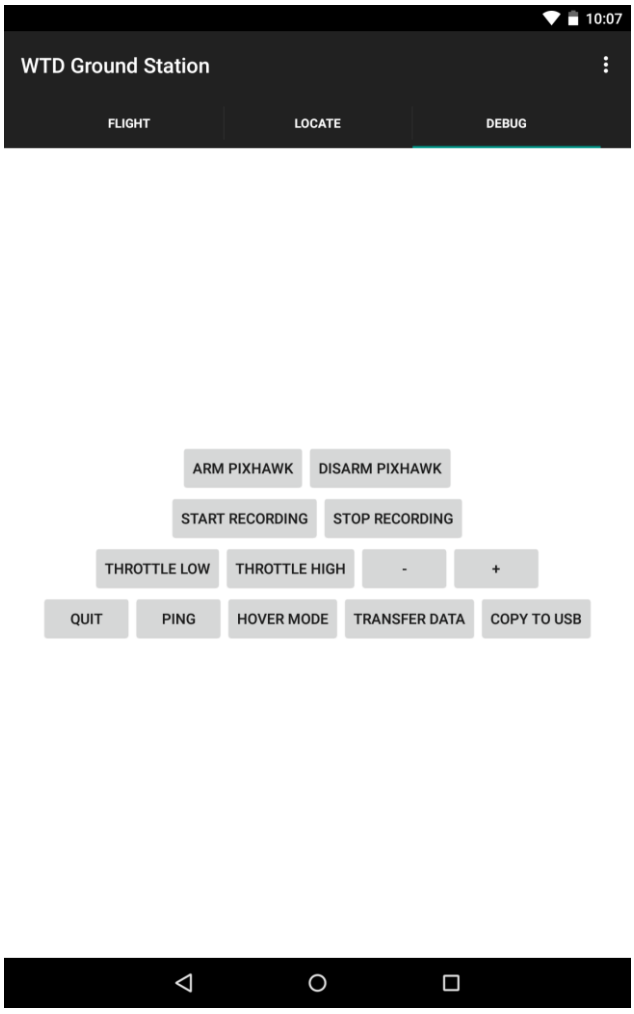

Figure 10. Screenshot of the ground station's debug screen.

All three components communicate with one another with the Raspberry Pi being the main hub as it is connected to the Pixhawk and the ground station but these two components are not connected to each other. An overview of this communication method and its different states can be seen in Figure 1 of Appendix B.

5.3 Telemetry

After an early consultation with Dr. David Dalton, we found that his team uses three different antenna styles in conjunction, which are two, three, and five-element Yagi antennae. Dr. Dalton's reasoning was that doing so provides a more predictable location of the bats. Figure 11 below illustrates the differences between the gains of the different antennae. Adding more elements will proportionally narrow and lengthen the beam width, which produces a more accurate reading during triangulation.

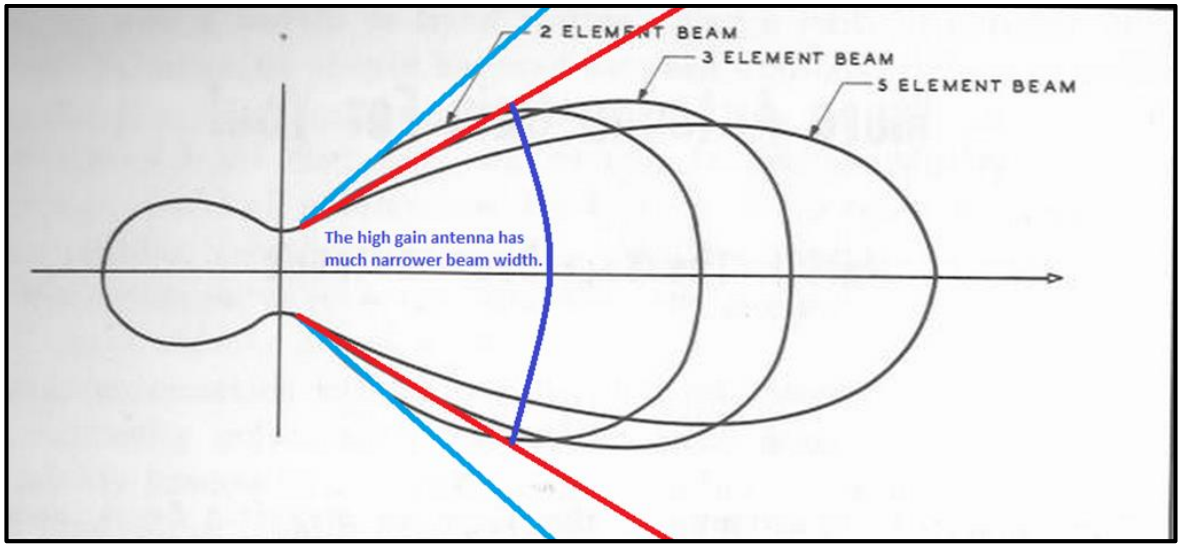

Figure 11. Antenna gain comparison [10].

5.3.1 H-Element Antenna or Two-Element Yagi

The two-element Yagi antenna is the smallest amongst the numerous Yagi element derivations. This type of antenna is significantly lighter in weight and smaller in size when compared to other Yagi antennae, but it lacks capabilities of receiving long-distance signals. Figure 12 below shows the configuration and azimuth plot (angular measurement in a spherical coordinate system) for this antenna. The azimuth plot displays the beam width and length of the antenna's reception.

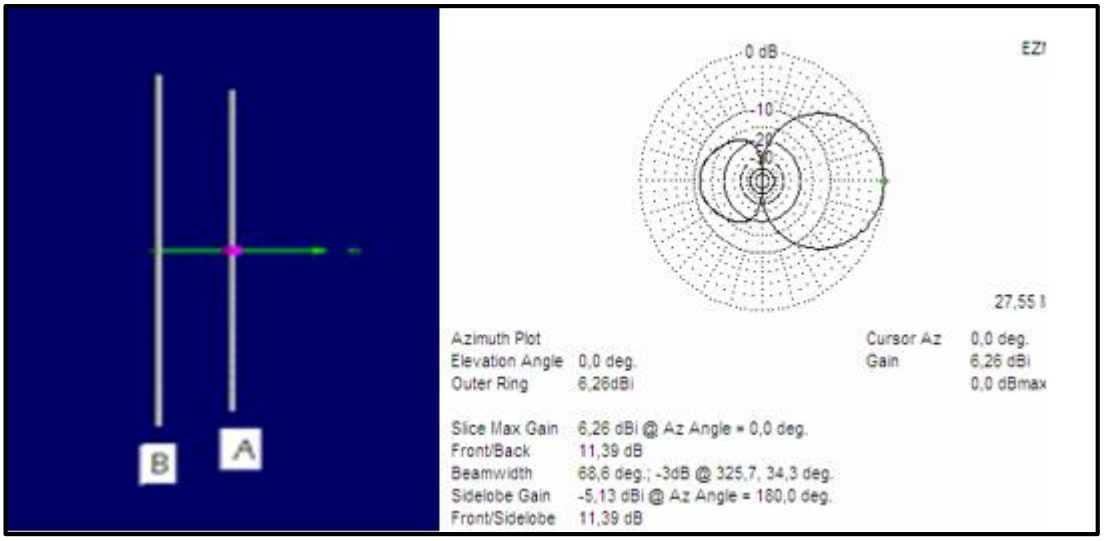

Figure 12. H-element Yagi antenna with azimuth plot.

5.3.2 Three-Element Yagi Antenna

The three-element antenna provides a lot more gain when compared to the two-element Yagi, at the expense of being less compact. In contrast, the three-element antenna has a similar beam width but a greater beam length, giving it a more directional azimuth plot as shown in Figure 11 above and Figure 13 below.

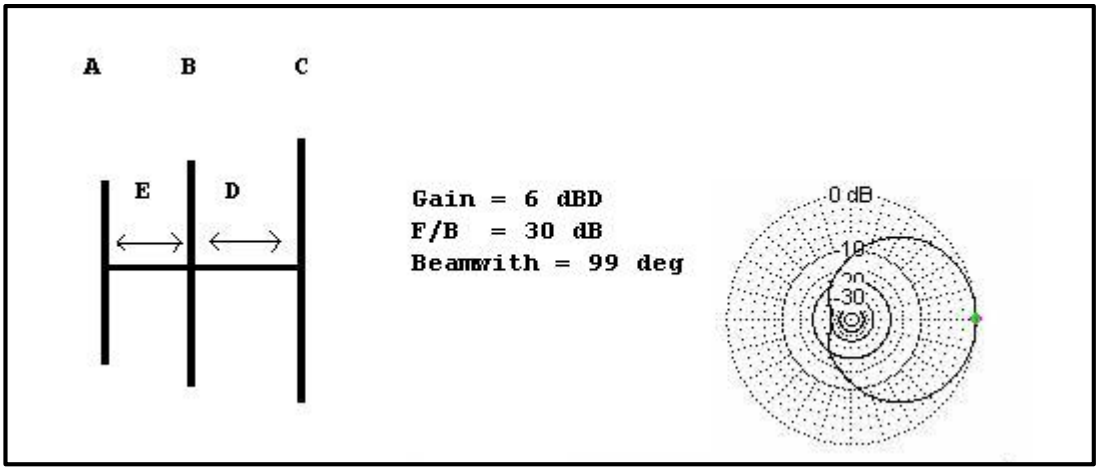

Figure 13. Three-element Yagi antenna with azimuth plot.

5.3.3 Five-Element Yagi Antenna

The five-element antenna provides the largest gain. Although this antenna may be lengthy, it allows for more precise signal receiving capabilities as shown on the azimuth plot in Figure 14.

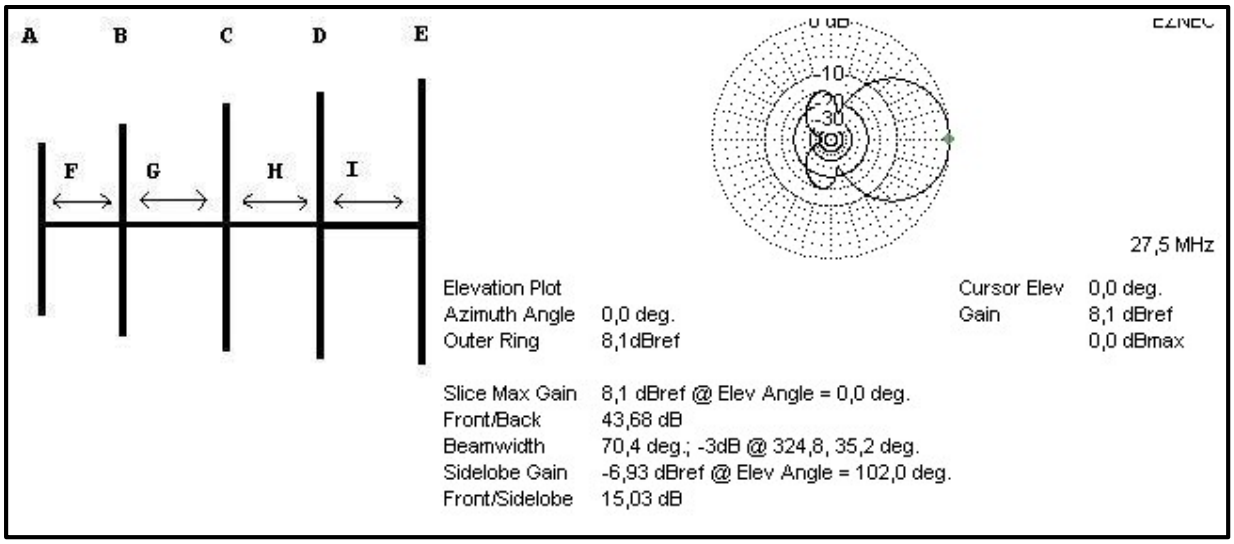

Figure 14. Five-element Yagi antenna with azimuth plot.

5.3.4 Final Antenna

After speaking with other field and scientific researchers, biologists, and hobbyists, and undergoing our own research, it became clear that the five-element antenna would be our best choice. However, due to our constraints on length and weight, we deemed it impractical. Therefore the decision was clear that we needed to go with the second most effective configuration, which is the three-element antenna. This provides us the capability of adequate signal range and therefore a more precise location when utilizing triangulation, while lessening the payload, and in turn increasing flight time.

With this in mind, we created the antenna shown in Figure 15 below in collaboration with the mechanical team, who ensured that it is durable, collapsible, lightweight, and includes predictable failure points for easy repair in the event of a crash.

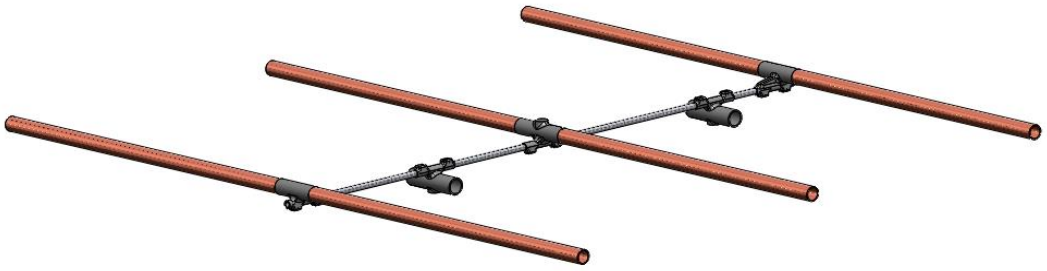

Figure 15. Final antenna modelled in CAD.

This design uses a carbon fiber boom to lighten the antenna while still providing a rigid attachment point, and 5/8” copper tubing for the elements. The spacing and element lengths were derived from the equations shown in Figure 16 below.

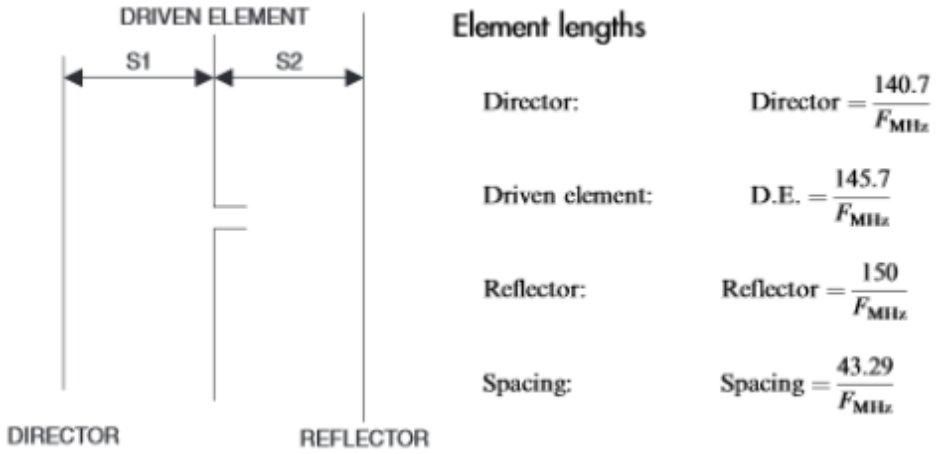

Figure 16. Equations for element lengths and spacing.

The antenna is also collapsible. The antenna in its disassembled form can be seen in Figure 17 below.

Figure 17. Final antenna in its collapsed, backpackable form.

5.3.5 Receiver

A receiver is a device that is able to hone in on different frequencies and provide the user with a tone when it senses the desired frequency. By aligning themselves with the direction from which this tone is loudest, the user is directed towards the transmitter and/or other devices in operation in the same frequency band. The requirements we are observing are as follows: frequency range of 148.xxx -152.xxx MHz, lightweight, and Raspberry Pi B+ compatible. The receiver must also be able to function without direct contact with the operator, since it will be mounted on a flying drone.

Currently, our client is using an R-1000 receiver for wildlife telemetry. However, this particular model is not ideal for use on a drone due to its lack of auto-adjusting gain or any sort of output besides raw audio data. The R-1000 receiver is shown in Figure 18 below.

Figure 18. R-1000 telemetry receiver [11]

We used the R-1000 in our design due to budget constraints, but it must be stressed that doing so introduces its own problems. The R-1000 is clearly a handheld design, and not optimized for a drone. With this design, the user is intended to manually adjust the gain as necessary during tracking, which is not possible while the receiver is mounted on the drone. As a result, the additional noise introduced by leaving the gain at a higher than necessary value must be later dealt with by extensive filtering. In addition, to even capture audio data in a usable format, a 3.5mm-to-USB adapter is necessary to connect the R-1000 to the Raspberry Pi, which introduces its own interference.

To avoid all of the issues discussed above, we strongly recommend that a receiver better suited to this design is added in the future. One example of such a receiver that we found appropriate is the Lotek Biotracker, shown in Figure 19 below. It is waterproof, works in a

wider range of frequencies (138-174 MHz), compact and light, especially if powered by our on-board battery rather than the included battery pack.

Figure 19. Lotek Biotracker receiver [12]

5.3.6 Filtering

Regardless of the antenna and receiver configuration, there will be some form of noise and/or interference introduced to the telemetry system. This noise will be increased by factors such as:

- Components operating at an interfering frequency (Pixhawk, Raspberry Pi, even the battery to some extent)
- Components that act as antennae (any unshielded wire or conductive plate)
- Objects between the telemetry system and the targeted transmitter (trees, rocks, buildings, etc.)

Reducing noise and interference was a central goal of this project, and the primary reason we used a drone for our design, as the third listed factor can be mostly eliminated by flying above the treeline. However, despite our best efforts, some noise remains in our received signal. This issue was amplified by the fact that, due to budget constraints, we used an analog receiver with an adapter, forcing us to work with raw audio data that is full of Gaussian noise.

To combat these issues, we created a Butterworth band-pass filter, which filters out all frequencies not in the specific range we are seeking. An example of signal data before and after the use of this filter can be seen below.

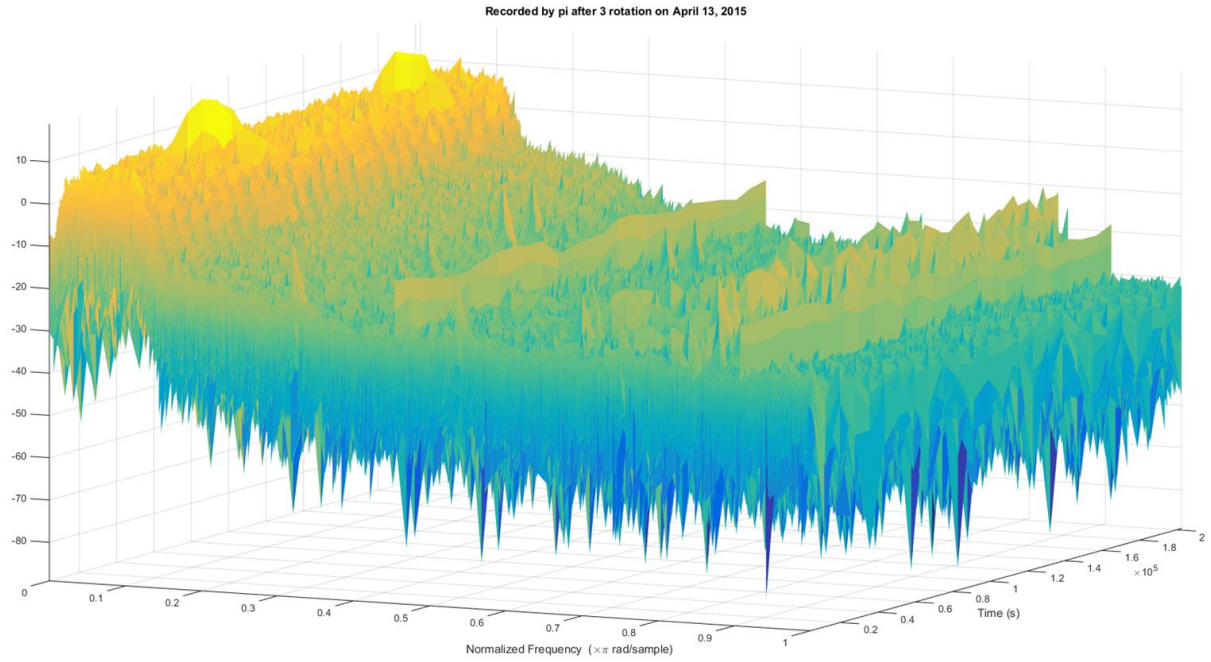

Figure 20. Signal data before filtering.

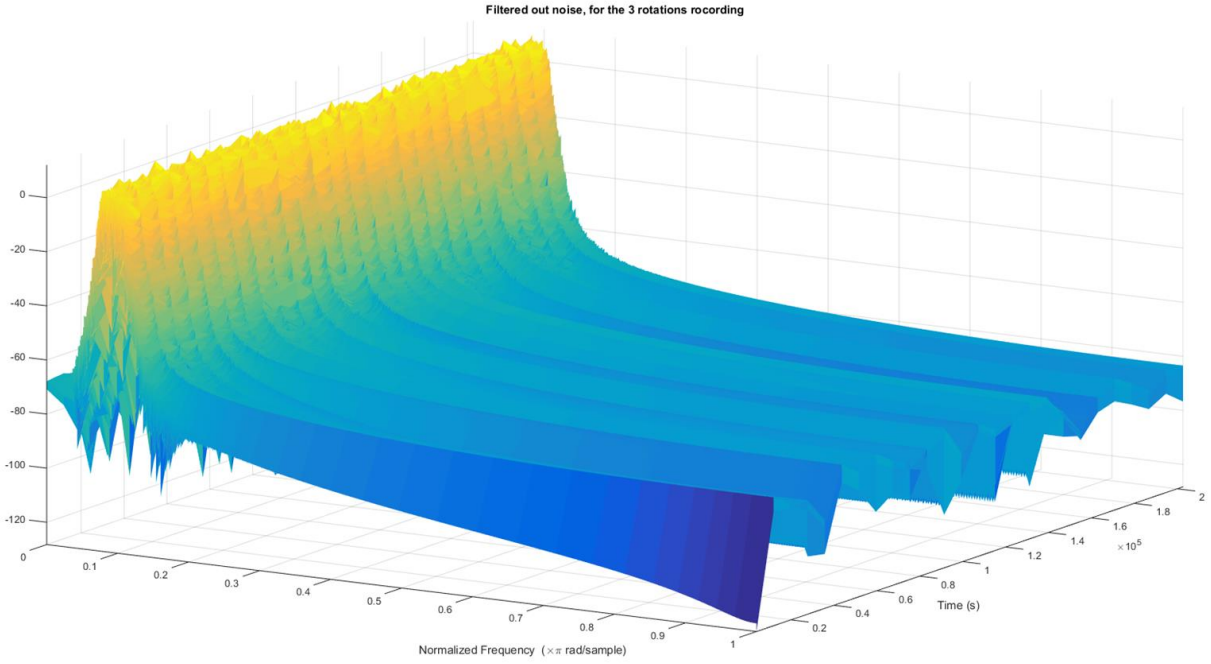

Figure 21. Signal data after Butterworth filter.

6. ITEMIZED BUDGET

There are two relevant budget reports that have been created during the course of this project.

The first is an estimated budget that was created early in the semester before a meeting with the Dean of the College of Engineering in which we attempted to gain funding, since at the time we only had $500 to use for a project that was estimated to need over $2,000 in parts. This will be shown in Figure 1 of Appendix C. We ended up receiving $2500 more in funding from Dr. Shafer and Dr. Flikkema. The respective contributions to our final budget can be seen in Figure 2 of Appendix C.

The second is the final expense report, which consists of all the purchases that were made throughout the project. This will be shown in Figures 3 through 5 of Appendix C. There is a significant difference between the estimated budget and the expense report for the telemetry team. We estimated that the telemetry team would spent the most by far, because the receiver is the most expensive aspect of the project. However, the receiver that we found best for this project ended up being too expensive for our budget, costing about $2,400. As a result, we decided to work with a receiver given to us by the NAUFD, which made the telemetry team's budget miniscule in comparison. A comparison between the estimated and final budget for each subteam can be found in Figure 6 of Appendix C.

7. CONCLUSION, RESULTS, AND THE FUTURE

At the conclusion of this project, a functional prototype has been created which fulfills the following specifications:

- Takes off and land vertically at the same point (within an area of 5 m)
- Easily fits in a hiking backpack (approximately 50x30x30 cm)
- Can sustain a drop of five feet while keeping systems operational and breaking only predicted, replaceable failure pieces
- Complies with FCC (Federal Communication Commission) and FAA (Federal Aviation Administration) regulations
- Accurately outputs a signal amplitude and GPS pairing according to telemetry data
- Allows signal and direction data to be transferred to an external device
- Allows for manual override of autonomous flight systems

The fully assembled final drone can be seen in Figure 22 below.

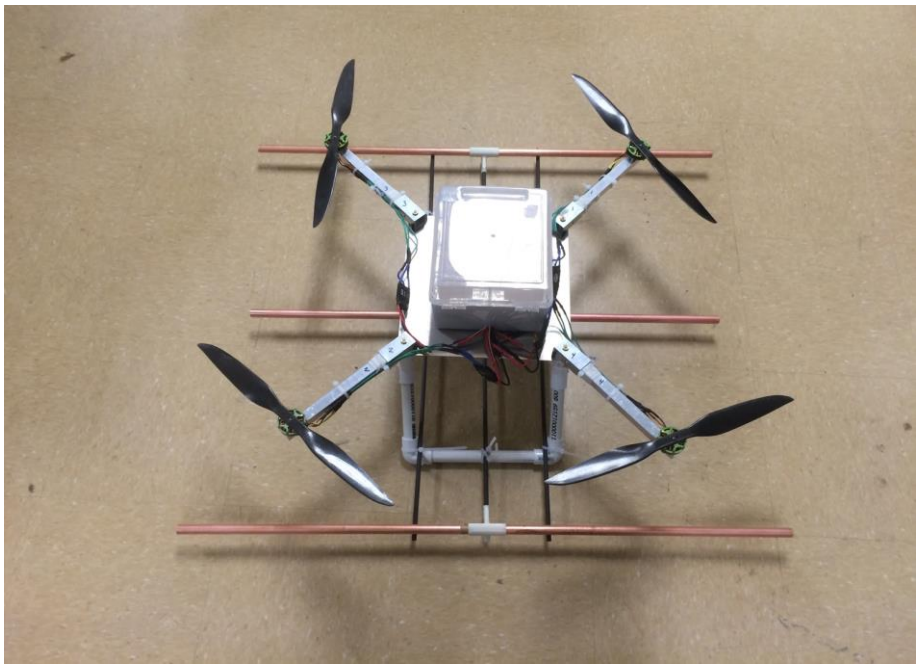

Figure 22. Completed wildlife telemetry drone.

This system can fly vertically into the air, spin 360 degrees while recording telemetry data and GPS coordinates, and offload that data to an external computer for filtering and display. The avionics and telemetry teams collaborated to create code to accomplish this, and an example graph of signal amplitude over time can be seen in Figure 23 below.

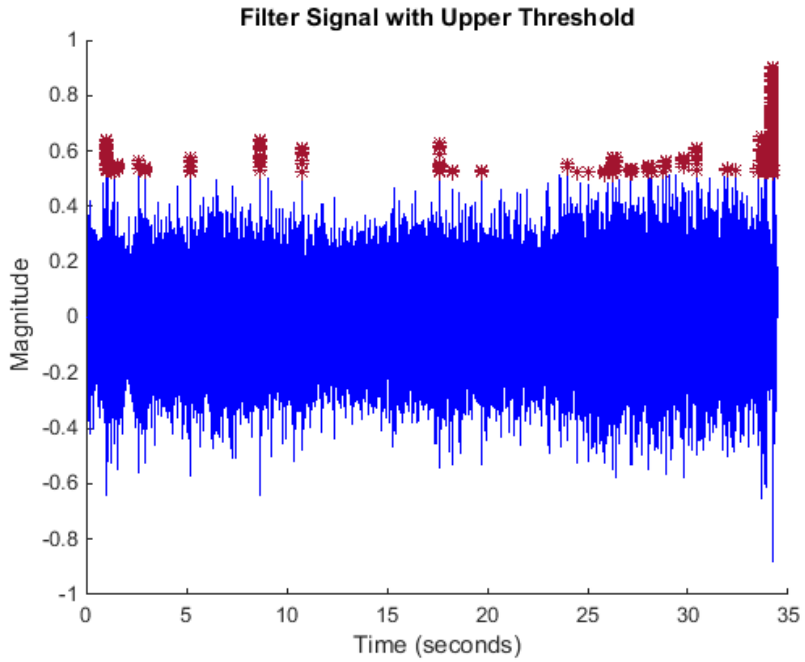

Figure 23. Filter signal data plotted with respect to time.

From this data, the greatest amplitude and time can be determined using MATLAB's sorting functions. An example MATLAB output can be seen in Figure 24 below demonstrating this.

```
The maximum magnitude is 0.906524, which occured at 34.2625 seconds
```

Figure 24. MATLAB output of magnitude and time data.

Finally, this data can be matched with the corresponding GPS coordinate at that time to give a heading of the bat's location. This overall process is effective, and serves to show that a wildlife telemetry drone can be a useful tool for researchers in locating tagged bats. However,

this system is far from perfect. In order to improve the usability and effectiveness of this design, we would recommend adding a digital receiver with auto-adjusting gain and a digital output. We would also recommend a non-conducting frame to reduce both weight and electromagnetic interference from the frame itself. Finally, we would recommend the implementation of long-range digital communication, so that long-range override is possible without the use of an additional RC controller.

With the basic design complete, future testing and system refinements should lead to a well-developed, functioning tool to aid in research of animal habitats and roosting patterns, while providing a foundation for future projects of a similar nature.

REFERENCES

[1] L. Meier. “MAVLink Documentation.” Internet: https://github.com/mavlink/mavlink [Nov. 21, 2014].

[2] 3DRobotics. “Communicating with Raspberry Pi via MAVLink.” Internet: http://dev.ardupilot.com/wiki/raspberry-pi-via-mavlink/ [Nov. 10, 2014].

[3] “UAV Dev Board.” Internet: https://code.google.com/p/gentlenav/, Jul 22, 2013 [Nov. 19, 2014].

[4] T. Hubing and N. Hubing. “Practical Electromagnetic Shielding.” Internet: http://www.learnemc.com/tutorials/Shielding02/Practical_Shielding.html [Sep. 29, 2014].

[5] R. Brigham. “Transmitter attachment for small insectivorous bats.” Internet: http://www.holohil.com/bd2att.htm, [Oct. 14, 2014].

[6] David Dalton. Sr. Systems Design Engineer, Photometrics. Interview. Tucson, AZ. October 6, 2014.

[7] “Aluminum Distributor ver. 11.” Internet: http://www.aerospacemetals.com/aluminum-distributor.html [Nov. 21, 2014].

[8] “Pixhawk Overview.” Internet: http://copter.ardupilot.com/wiki/common-autopilots/common-pixhawk-overview [Nov. 10, 2014].

[9] “Raspberry Pi Model B+.” Internet: http://www.cnet.com/uk/products/raspberry-pi-model-b-plus/ [Nov. 10, 2014].

[10] “Antenna Types – Yagi.” Internet: http://www.cbantennaguide.com/Yagis.htm [Nov. 21, 2014]

[11] “Comunications Specialists R-1000 Telemetry Handheld Receiver.” Internet: http://www.awt.co.za/awt_accessories/accessories.htm [Nov. 21, 2014].

[12] “Biotracker.” Internet: http://www.lotek.com/biotracker.pdf [Nov. 21, 2014].

[13] J. Seddon, S. Newman. Basic Helicopter Aerodynamics, 2nd ed. Reston, VA: AIAA, 2001.

APPENDIX A: THRUST ANALYSIS

The essential function of a propeller is to convert a shaft work input to a change in momentum for a stream of air, which in turn applies a force to some body. In the case of a quadcopter style drone, this thrust force is the means of producing lift to achieve flight. Understanding the principles for achieving thrust, then, is essential to selection of suitable components to achieve flight. The following is heavily sourced from Basic Helicopter Aerodynamics, Second Edition, by J. Seddon and Simon Newman, from the AIAA Education series. It is adapted to the specific application of power and thrust calculation for hobby propellers designed for remote control vehicles.

To begin modeling thrust from a propeller, let us begin by modeling the propeller itself as an actuator disk which a stream tube of air is passed through. We will assume incompressible, steady flow with uniform properties at the inlet and exit. We will also neglect gravitational effects.

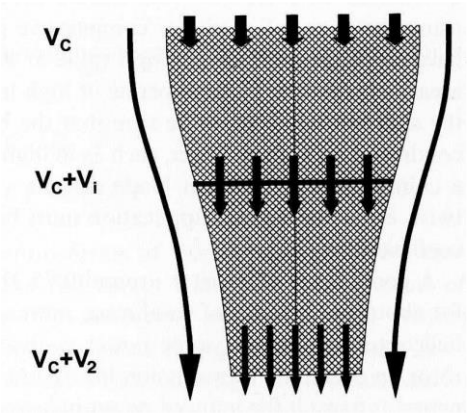

Figure 1. Side view of control volume, with actuator disk at location of bold line [13].

The thrust produced can be found using conservation of momentum, in the form of Reynolds Transport Theorem considering some section of the stream tube, which, through our assumptions simplifies to

$$T = \dot{m}v_e - \dot{m}v_0$$

where v_e and v_0 are the velocities at the exit and inlet respectively. Under our assumptions, the mass flow rate is constant and equivalent between any two locations in the stream tube. We evaluate the mass flow rate at the location of the actuator disk, introducing a new term v_i which is the velocity induced at the actuator disk which results from the work input there. Using this, the mass flow rate is

$$\dot{m} = \rho v_i A$$

where A is the area of the actuator disk, or the area of the circular plane in which the propeller spins. This yields

$$T = \rho v_i A(v_e - v_0)$$

The thrust produced by the actuator disk can also be modeled as

$$T = \Delta p_t A$$

Where Δp_t is the change in total pressure across the actuator disk. At this point, it is important to note that work is being done on the air flowing through the actuator disk, which results in an increase in kinetic energy of the flow. Because work is done to the flow, Bernoulli's theorem cannot be used to describe the flow through the disk, only on either side separately. Applying Bernoulli's theorem on the flow upstream and downstream of the disk respectively we find

$$p + \frac{1}{2}\rho v_0^2 = p + \frac{1}{2}\rho v_i^2$$

and

$$p + \frac{1}{2}\rho v_i^2 + \Delta p_t = p + \frac{1}{2}\rho v_e^2$$

Note Δp_t which comes due to the work done on the flow through the disk. Simplifying these, substituting, and solving for Δp_t we find

$$\Delta p_t = \frac{1}{2}\rho (v_e^2 - v_0^2)$$

Plugging into our thrust equation from earlier

$$T = \frac{1}{2}\rho A (v_e^2 - v_0^2)$$

Then setting our two trust equations equal to one another, and simplifying

$$\frac{1}{2}\rho A (v_e^2 - v_0^2) = \rho v_i (v_e - v_0)$$

$$2v_i = v_e + v_0$$

Noting that at some point far upstream of the actuator disk the velocity is very close to zero, we find that

$$v_0 \approx 0$$

Therefore

$$2v_i = v_e$$

Applying this new information and the assumption of zero velocity far upstream to our first thrust equation we find that

$$T = 2\rho A v_i^2$$

Solving for the induced velocity v_i

$$v_i = \sqrt{\frac{T}{2\rho A}}$$

This induced velocity is useful as we introduce blade element theory, as it affects the angle of attack for the airfoil shape of some blade element. We will consider a blade element with width dy and chord length c, at some location y along the span of a blade with radius R, spinning at angular velocity Ω as shown in Figures A2 and A3 below.

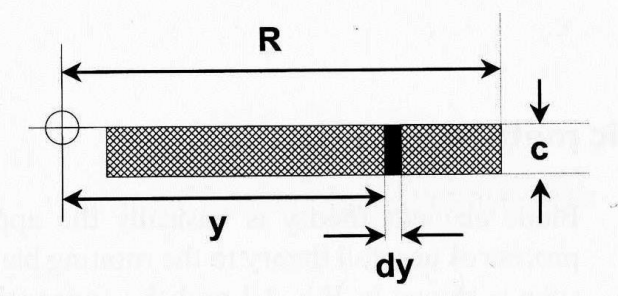

Figure A2. Blade strip coordinates [13].

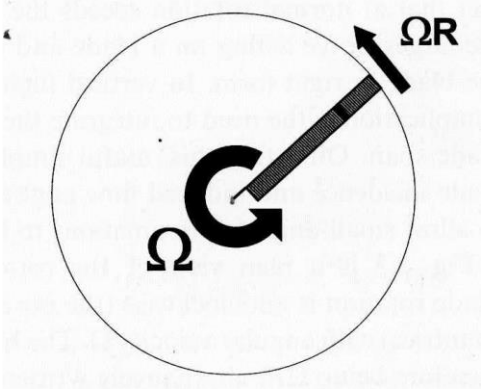

Figure A3. Propeller disc viewed from above [13].

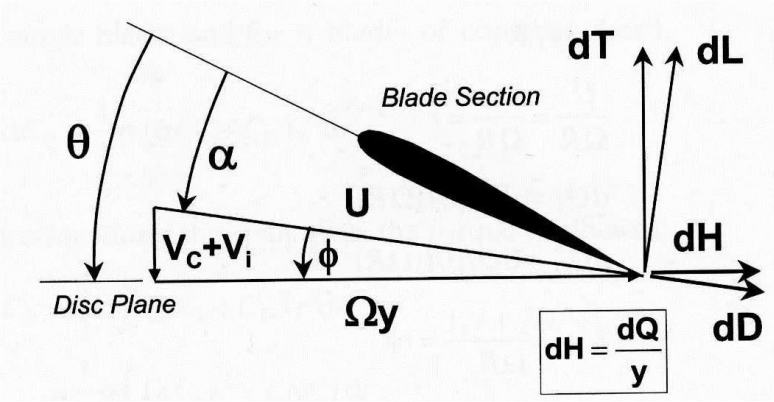

Figure 4. Blade element flow conditions and forces [13].

Here, θ is called the pitch angle, seen in Figure 4. This is not to be confused with the *pitch* of a propeller (we'll call it M), which results from the pitch angle of a propeller and can be understood as the distance a propeller would travel forward through a solid substance during a

360° rotation. The angle the velocity vector is tilted by the downward velocity is called ϕ. We can see that

$$\phi = tan^{-1}\left(\frac{v_i + V_c}{\Omega y}\right)$$

$$U = \frac{\Omega y}{cos\phi}$$

$$dL = \frac{1}{2}(\rho U^2 c C_L)dy$$

$$dD = \frac{1}{2}(\rho U^2 c C_D)dy$$

$$dT = dL\, cos\phi - dD\, sin\phi$$

$$dQ = (dL\, sin\phi + dD\, cos\phi)y$$

Noting that V_c is the vehicle's vertical velocity. Generally, ϕ is assumed to be small, and so we continue using small angle approximations.

$$\phi \approx \frac{v_i + V_c}{\Omega y}$$

$$U \approx \Omega y$$

$$dT \approx dL$$

$$dQ \approx (\phi dL + dD)y$$

At this point it is convenient to nondimensionalize our terms. We begin with r which can be seen to be a percentage of the radius R of the blade.

$$r = \frac{y}{R}$$

This also arises as the result when we nondimensionalize the velocity U with the tip velocity ΩR.

$$r = \frac{U}{\Omega R} = \frac{\Omega y}{\Omega R}$$

Now we find a differential coefficient of thrust dC_T, and differential coefficient of torque dC_Q

$$dC_T = \frac{dT}{\rho A(\Omega R)^2}$$

$$dC_Q = \frac{dQ}{\rho A(\Omega R)^2 R}$$

We may also use tip velocity to nondimensionalize the induced velocity through the plane of the propeller.

$$\lambda = \frac{v_i + V_c}{\Omega R} = \left(\frac{v_i + V_c}{\Omega y}\right)\left(\frac{\Omega y}{\Omega R}\right) = \phi r$$

For simplicity, we will continue our analysis for the hover condition, where $V_c = 0$, therefore

$$\lambda = \frac{v_i}{\Omega R}$$

If we substitute the quantity previously determined for dT into our equation for dC_T we find

$$dC_T = \frac{\frac{1}{2}\rho U^2 c C_L dy}{\rho(\pi R^2)(\Omega R)^2}$$

Which simplifies to

$$dC_T = \frac{1}{2}\frac{c}{\pi R} C_L r^2 dr$$

It is convenient to introduce a new term σ, called the solidity factor defined as

$$\sigma = \frac{NcR}{\pi R^2} = \frac{Nc}{\pi R}$$

Where N is the total number of blades. This means σ can be seen as the ratio between the total blade area and the disk area of the propeller. This allows us to simplify our dC_T equation, for a single blade, to

$$dC_T = \frac{1}{2}\sigma C_L r^2 dr$$

Which we may integrate to get

$$C_T = \frac{1}{2}\sigma \int_0^1 C_L r^2 dr$$

Similarly, we can find

$$dC_Q = \frac{1}{2}\frac{c}{\pi R}(\phi C_L + C_D) r^3 dr$$

Which our solidity factor is also useful for, and may be integrated as well

$$C_Q = \frac{1}{2}\sigma \int_0^1 (\phi C_L + C_D) r^3 dr$$

This result can be simplified using λ to get

$$C_Q = \frac{1}{2}\sigma \int_0^1 (\lambda C_L r^2 + C_D r^3) dr$$

Assuming a symmetric airfoil shape C_L can be found with

$$C_L = a * \alpha$$

Where α is angle of attack and a is the constant lift curve slope ($a = 2\pi$ is generally a very good approximation for airfoils, however the book here recommends $a = 5.7$) which, in this case, results in

$$C_L = a(\theta - \phi)$$

Note that this assumes a symmetric airfoil shape, which will most likely under approximate the thrust produced. Substituting this into our C_T integral we get

$$C_T = \frac{1}{2}\sigma a \int_0^1 (\theta r^2 - \lambda r) dr$$

Which evaluates to

$$C_T = \frac{1}{2}\sigma a \left(\frac{1}{3}\theta - \frac{1}{2}\lambda\right)$$

So far, we have assumed θ and λ to be constants. This assumption, however, is poor. Let us consider the differential form of the equation for dC_T and a differential form of the thrust equation found from momentum theory

$$dT = 2\rho v_i^2 dA$$

Which can be nondimensionalized to

$$dC_T = 4\lambda^2 r\, dr$$

When we set the two equal to one another, we find a quadratic equation for λ whose solution is a function of r as given below.

$$\lambda = \frac{\sigma a}{16}\left(\sqrt{1 + \frac{32}{\sigma a}\theta r} - 1\right)$$

To more closely meet this assumption, we vary θ along the span of the blade. By introducing a linear twist of the blade along the span, in other words making the pitch angle vary linearly with the radius, we can reduce the errors introduced to less than a few percent. A convenient way to do this is to make the reference pitch at three quarters the radius of the blade, as such

$$\theta = \theta_{.75} + (r - 0.75)\theta_{tw}$$

Where $\theta_{.75}$ is the pitch angle at three quarters the radius and θ_{tw} is the rate of change of the pitch angle with r (θ_{tw} is a negative value). The convenience of doing this is that the result of integrating our differential coefficient of thrust equation with this substituted in for θ is the same. Due to the nomenclature for nominal dimensions of hobby propellers being the diameter in inches followed by the pitch at three quarters the radius, it is assumed throughout the rest of this analysis that hobby propellers use linear twist, based on this convention.

Now, recall that

$$v_i = \sqrt{\frac{T}{2\rho A}}$$

And

$$\lambda = \frac{v_i}{\Omega R}$$

Plugging v_i into λ, we can find that

$$\lambda = \sqrt{\frac{C_T}{2}}$$

Substituting this into our equation for coefficient of thrust, we obtain a quadratic equation for C_T. Noting that

$$\theta_{.75} = \arctan\left(\frac{4M}{3\pi D}\right)$$

Where M is the nominal pitch of the propeller and D is the diameter, the solution to the quadratic is as follows

$$C_T = \left(\frac{-\frac{3}{2\sqrt{2}} + \sqrt{\frac{9}{8} + \frac{12\pi D}{Nca}\arctan\left(\frac{4M}{3\pi D}\right)}}{\frac{6\pi D}{Nca}} \right)^2$$

Where N is the number of blades, c is the mean chord length of the blades, and a, remember, is the lift curve slope (5.7 here).

Let us revisit our equation for coefficient of torque, in order to develop a coefficient, which is more useful when finding suitable motors.

$$dC_Q = \frac{dQ}{\rho A(\Omega R)^2 R}$$

$$dC_Q = \frac{1}{2}\frac{c}{\pi R}(\phi C_L + C_D) r^3 dr$$

Noting that $P = \Omega Q$, it can be seen that C_Q and C_P are identical. Through some simple substitutions we can find that

$$dC_P = \lambda\, dC_T + \frac{1}{2}\sigma C_D r^3\, dr$$

Integrating yields

$$C_P = \lambda C_T + \frac{1}{8}\sigma C_{D_0}$$

Which simplifies further to

$$C_P = \frac{C_T^{3/2}}{\sqrt{2}} + \frac{1}{8}\sigma C_{D_0}$$

Where C_{D_0} is the coefficient of drag for the airfoil at zero angle of attack. Here, our assumption of uniform inflow yields much larger errors. To correct this, an empirically derived correction factor k is used which only affects the first term.

$$C_P = k\frac{C_T^{3/2}}{\sqrt{2}} + \frac{1}{8}\sigma C_{D_0}$$

During the development of a MATLAB code to calculate the maximum thrust produced by a given propeller, very little data had been acquired, for use of comparison, despite exhaustive research. This limited data set, however, did offer some insight for other possible considerations. When compared to the data sets, predictions showed much higher thrust produced with much lower power inputs to the system. To attempt to correct this, tip vortex effects were considered. A simple way to do this is to consider only a portion of the blades as producing lift but the entirety producing drag. This however means that the integral no longer simplifies so nicely. We change the limits of integration to

$$C_T = \frac{1}{2}\sigma a \int_0^B (\theta r^2 - \lambda r) dr$$

As well as changing the area to an effective area

$$A_e = \pi (BR)^2$$

Causing λ to become

$$\lambda = \frac{1}{B}\sqrt{\frac{C_T}{2}}$$

Which results in a coefficient of thrust equation

$$C_T = \left[\left(\frac{NcaB}{6\pi D} \right) \left(\frac{-3}{2\sqrt{2}} + \sqrt{\frac{9}{8} + \frac{12\pi DB \arctan\left({}^{4M}/_{3\pi D}\right) - 9\pi DB(1-B)\theta_{tw}}{Nca}} \right) \right]^2$$

And a coefficient of power equation

$$C_P = \frac{k}{B}\frac{C_T^{\,3/2}}{\sqrt{2}} + \frac{1}{8}\sigma C_{D_0}$$

Using a value of $B = .85$ corrected the thrust predictions, however, power input predictions were still far lower than the data indicated. Part of the issue is the lack of detailed information regarding C_{D_0} or which airfoil is used. Because of this, the second term is accounted for using a multiplier in front of the first term. While the multiplier can be manipulated to help best fit the data set, values which do so are much larger than expected. This suggests that there may be an assumption made in the derivation of the coefficient of power, which does not hold up well for propellers with smaller nominal dimensions.

Concerns could arise from some of the later statements regarding corrections done to help fit a sparse data set. While the data set is sparse, all corrections were aimed to underestimate thrust and over approximate power. Keeping this in mind, a design resulting from this analysis should be, at worst, more than capable of doing what is required of it.

```
%propB.m
%Predicts maximum thrust produced and power required for a given propeller
%Written by Alex Moore
%last revision 11/7/14

function [T,P,Om]=propB(D,M,KV,V)
%Takes inputs of Diameter, D, and Pitch, M, in inches, motor KV rating, and
%battery voltage to output graph of thrust as a function of power

%constants
rho = 1;        %kg/m^3 air density
a = 5.7;        %lift curve slope
N = 2;          %number of blades
c = .08*D;      %assumed chord length as a percentage of diameter
B = .85;        %assumed percent of blade span producing lift
tw = -pi/9;     %linear twist slope (based on a 10" diameter prop with 10deg
pitch angle at tip and 30deg pitch angle at root)
%unit conversions
D = .0254*D;    %m
M = .0254*M;    %m
c = .0254*c;    %m
%Coeff. of thrust
CT = (((-3/(2*sqrt(2)))+sqrt((9/8)+((12*pi*D*B*atan(4*M/(3*pi*D))-
9*pi*D*B*(1-B)*tw))/(N*c*a)))*(N*c*a*B/(6*pi*D)))^2;
%Coeff. of power
CP = 1.25*(4/(B*3))*(1.15/sqrt(2))*CT^(3/2);    %includes a fudge factor of
1.25
%CP = (4/(3))*(1.15/sqrt(2))*CT^(3/2);
%Possible rpm range of motor
F = (0:100:(KV*V));             %rpm
Om = (2*pi/60).*F;              %rad/s
T = (CT*pi*rho*D^4/16).*Om.^2;  %N
P = (CP*rho*pi*D^5/32).*Om.^3;  %W
%unit conversions
T = .22481.*T;                  %lbs
%T = T./9.81;                    %kg
plot(P,T);
end
```

```
%PropTest.m
%Script to run prop function and compare to presented data
%Written by Alex Moore
%last revision 11/6/14

%input data provided online from hobbyking.com for NTM multirotor motors
data = [8   4   800     22.2    310     1.11
8   4   900     14.8    159     0.75
8   4   1100    11.1    100     0.54
8   4   1100    14.8    116     0.82
9   6   900     11.1    120     0.68
9   6   900     14.8    234     1.05
9   6   1100    11.1    149     0.73
9   6   1100    14.8    285     1.05
10  5   800     18.5    315     1.27
10  5   900     11.1    133     0.75
11  7   800     14.8    260     1.05
11  7   900     11.1    188     0.89
12  6   800     14.8    276     1.2
12  6   900     11.1    195     1.01
13  4   900     11.1    194     1.04];
%Initialize matrices for theoretical and calculated Coeff. of Thrust
CT = [];
CTR = [];
for i = 1:15
    k = propB(data(i,1),data(i,2),data(i,3),data(i,4));
    CT = [CT;[data(i,1),k]];
    k2 =
(16*9.81*data(i,6))/(pi*(.0254*data(i,1))^4*(data(i,3)*data(i,4)/2)^2);
    CTR = [CTR;[data(i,1),k2]];
    %collect desired outputs from results
    %need to make T and P outputs of function and collect corresponding
    %outputs
end
plot(CT(:,1),CT(:,2));
hold on
plot(CTR(:,1),CTR(:,2));
%calculate difference between calculated and actual
E = CT(:,2)-CTR(:,2);
```

APPENDIX B: Avionics State Machine

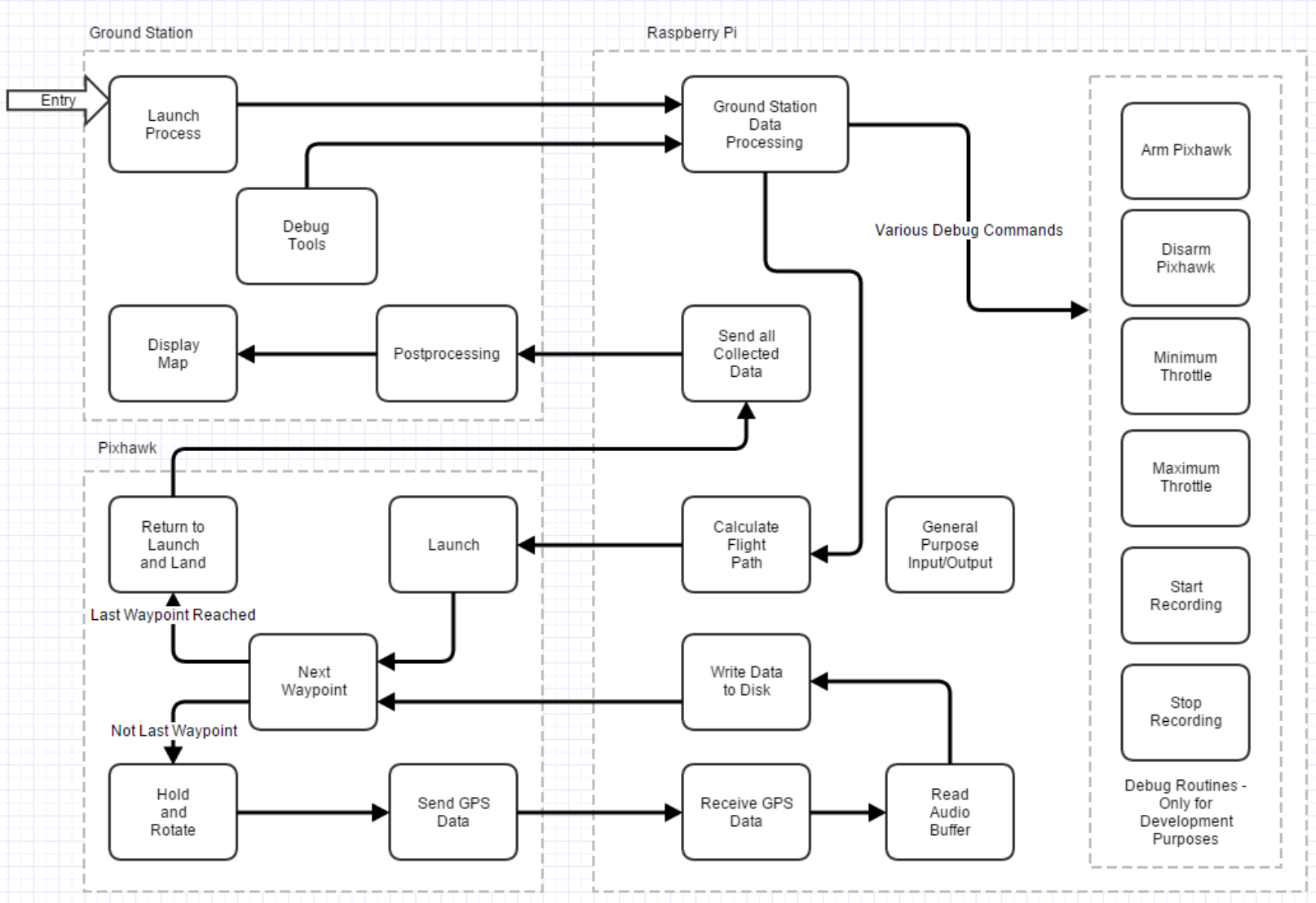

Figure B1. State Machine for Drone Control Systems

APPENDIX C: Budget and Expense Reports

Drone team estimated budget for drone

Mechanical

Component	Description	Quantity	Price	Total
Aluminum Arms	1"x1" 1/8" thick Square Tubing	4ft	$30.00	$30.00
Base Plate	Machined 6061 Aluminum Plate 8"x8"x1/8"	2	$48.34	$96.68
Foam	Foam Padding 12"x12"x3/4"	2	$17.44	$34.88
Fasteners	Miscellaneous Bolts and Connectors	As Needed	$20.00	$20.00
Plastic Pins	Failure Component - Weak Link in Arm Structure	TBD	$10.00	$10.00
Machining Costs	Machining of Base Plate and Arms	N/A	$50.00	$50.00
Buffer	Spare parts, unforeseen costs, and telemetry		$100.00	$100.00
				$341.56

Avionics

Component	Description	Quantity	Price	Total
Motor	850KV 311W brushless outrunner	4	$20.35	$81.40
ESC	30A 2-4S	4	$14	$56.00
Propellers	17" carbon fiber	1	$39.97	$39.97
Battery	8400mAh 3S1P 30C	1	$64.05	$64.05
Telemetry	3DR radio set with micro USB	1	$100.00	$100.00
Charger	2S/3S Lipo charger	1	$12.35	$12.35
Flight Controller	PixHawk and GPS module	1	$279.98	$279.98
Bluetooth	Class 1 (~100M) dongle	1	$14.99	$14.99
Board	Raspberry Pi B+ kit	1	$69.99	$69.99
Board Battery	5V 5600 mAh USB charger	1	$9.99	$9.99
Buffer	Spare parts, unforeseen costs, and telemetry	1	$200.00	$200.00
				$928.72

Telemetry

Component	Description	Quantity	Price	Total
Antenna	Antenna	1	$230.71	$230.71
Reciever	AOR AR8200 Mark III B	1	$909.00	$909.00
USB Cable	USB8200 or USB 8200A	1	$99.00	$99.00
Coax Cabe	12BNSO	1	$5.95	$5.95
Buffer	Spare parts and unforeseen costs	1	$300.00	$300.00
				$1,544.66

Total	**$2,814.94**

Figure C1. Estimated Budget

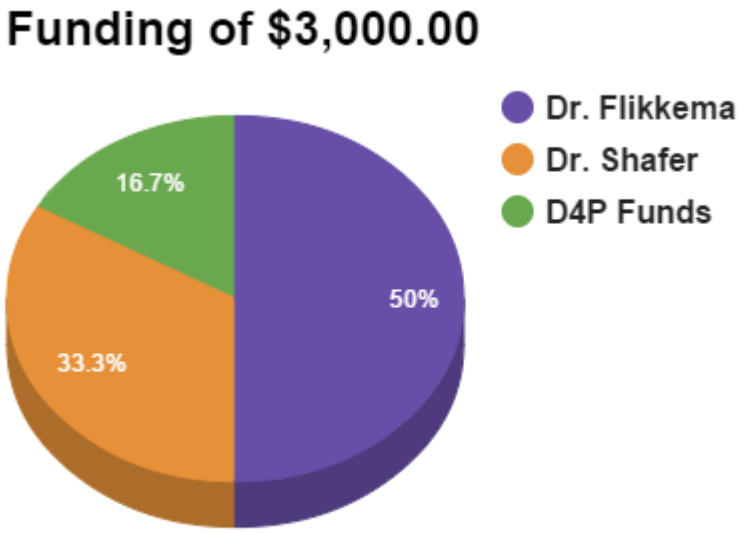

Figure C2. Funding contributions.

Mechanical				
Component	Description	Quantity	Price	Total
Motor	Turnigy Multistar 4220-880Kv 16Pole Multi-Rotor Outrunn	4	$22.95	$91.80
Speed controllers	Turnigy Multistar 20 Amp Multi-rotor Brushless ESC 2-4S	4	$9.75	$39.00
Rotor	16x4 Carbon Fiber propellers for DJI S800 L/H and R/H R	2 pair	$20.95	$41.90
Battery	Zippy Compact 5800mAh 3S 25C Lipo Pack	1	$45.96	$45.96
Charger	Turnigy E3 Compact 2S/3S Lipo Charger 100-240v (US pl	1	$12.35	$12.35
	Shipping Fee			$38.61
Motor	Turnigy Multistar 4220-880Kv 16Pole Multi-Rotor Outrunn	1	$22.95	$22.95
Rotor	16x4 Carbon Fiber propellers for DJI S800 L/H and R/H R	1	$20.95	$20.95
	shpping		$7.99	$7.99
ESC	New Turnigy Multistar 20 Amp 20a Multi-rotor Brushless E	2	$19.84	$39.68
	New Turnigy Multistar 20 Amp 20a Multi-rotor Brushless ESC 2-4S US		$9.00	$9.00
Motor	Turnigy Multistar 4220-880Kv 16Pole Multi-Rotor Outrunn	1	$22.95	$22.95
Power meter	HobbyKing® Compact 30A Watt Meter and Power Analyzer	1	$8.85	$8.85
	Shipping		$7.99	$7.99
Frame Purchases	Hard High-Strength 7075 Aluminum, 0.125" Thick, 8" by 8	1	$24.14	$24.14
Frame Purchases	Multipurpose 6061 Aluminum Rectangular Tube, 1/16" W	1	$15.56	$15.56
	Shipping			$26.51
Fasteners	Mach Screw 32x1-1/2	3	$1.18	$3.54
	tax		$0.29	$0.29
Plastic Box	Home organizer box	1	$9.94	$9.94
	tax		$0.89	$0.89
Fasteners	bolt, nut and screw mis box&bulk (4 invoices)	1	$9.33	$9.33
Fasteners	bolt, nut and screw mis box&bulk (4 invoices)	1	$13.82	$13.82
Base plate	hard high strength 7075 Aluminum .09" thick 12"x12"	1	$38.68	$38.68
Rectangular tube	Multipurose 6061 Aluminum Rectangular Tube 1/16" wall	1	$9.82	$9.82
Rectangular tube	Multipurose 6061 Aluminum Rectangular Tube 1/16" wall	1	$9.02	$9.02
Quick release button	zinc-plated steel quick- release button connectors	2	$4.08	$8.16
Frim gray f3 felt shee	1/8" Thick, 12" x 12" adhesive back	1	$13.51	$13.51
	shipping			$19.54
				$612.73

Figure C3. Mechanical Final Expense Report.

Avionics				
Component	**Description**	**Quantity**	**Price**	**Total**
Pixhawk	3DR Pixhawk	1	$199.99	$199.99
GPS	3DR uBlox GPS with compass kit	1	$79.99	$79.99
	Shipping			$4.12
Raspberry Pi	CanaKit Raspberry Pi B+ Ultimate starter kit	1	$69.99	$69.99
USB Bluetooth adapt	Azio BTD-V201 USB Micro Bluetooth Adapter, Class 1	1	$12.99	$12.99
	Tax			$1.08
PPM	Encoder	1	$24.90	$24.90
	shipping		$6.00	$6.00
Mermory Card	Card W/ adapter 45MB/s	1	$8.95	$8.95
	tax		$1.79	$1.79
	Shpping		$11.04	$11.04
Battery	5000 amp/h 3 cel battery	1	$65.36	$65.36
USB	USB extension cable	1	$14.97	$14.97
	tax			$1.34
Bullet connectors	gold blt conn male & female 3.5mm	8	$24.61	$24.61
RC controller	Receiver(mode 1)(v2 firmware)+shipping	1	$144.06	$144.06
Pixhawk ESC	ESC 20 amp with Simonk	4	$25.99	$103.96
Power connectors	XT60 connector male & female	2	$1.25	$2.50
	shipping			$2.68
Programming tool	ESC Progamming Tool	1	$7.85	$7.85
	shipping			$6.69
				$794.86

Figure C4. Avionics Final Expense Report.

Telemetry				
Component	**Description**	**Quantity**	**Price**	**Total**
Base of antenna	36"X3/4"X 1/16" ALUMINUM SQUARE TUBE	1	$11.47	$11.47
Drill	MILWAUKEE 5/16" BLK OXIDE DRILL BIT	1	$4.37	$4.37
Antenna parts	36"X1/4" ROUND ROD ALUMINUM (Three rods)	1	$12.63	$12.63
	Tax			$2.37
Antenna rod	2011-T3 Aluminum Round Rod .25" Dia Cold Finish 3ft	1	$2.18	$2.18
Antenna rod	2011-T3 Aluminum Round Rod .25" Dia Cold Finish 4ft	2	$2.60	$5.20
	Shipping Fee			$13.27
Aluminum screen	Tester to make a fraday's case	1	$13.01	$13.01
Shielding	Foil Tape 50yd	1	$7.88	$7.88
	tax		$0.71	$0.71
AUX cord	3' 1/8 M-M patch cable or AUX cord	1	$4.99	$4.99
	tax			$0.45
Wires	black & red wires 10ft 14 awg solid	2	$2.00	$4.00
Tape Mounting	Exterior Mounting Tape	1	$4.97	$4.97
Tubing	Black Flex Tubing	1	$2.48	$2.48
	tax		$1.02	$1.02
Velcro	Velcro 5 PK	1	$4.47	$4.47
Spray paint	Spray Paint	1	$3.86	$3.86
	tax			$0.75
Boom/mounting rod	Carbon Fiber Arrows	6	$35.00	$35.00
	tax			$3.13
				$138.21
			Total	**$1,545.80**

Figure C5. Telemetry Final Expense Report and Total Expenses.

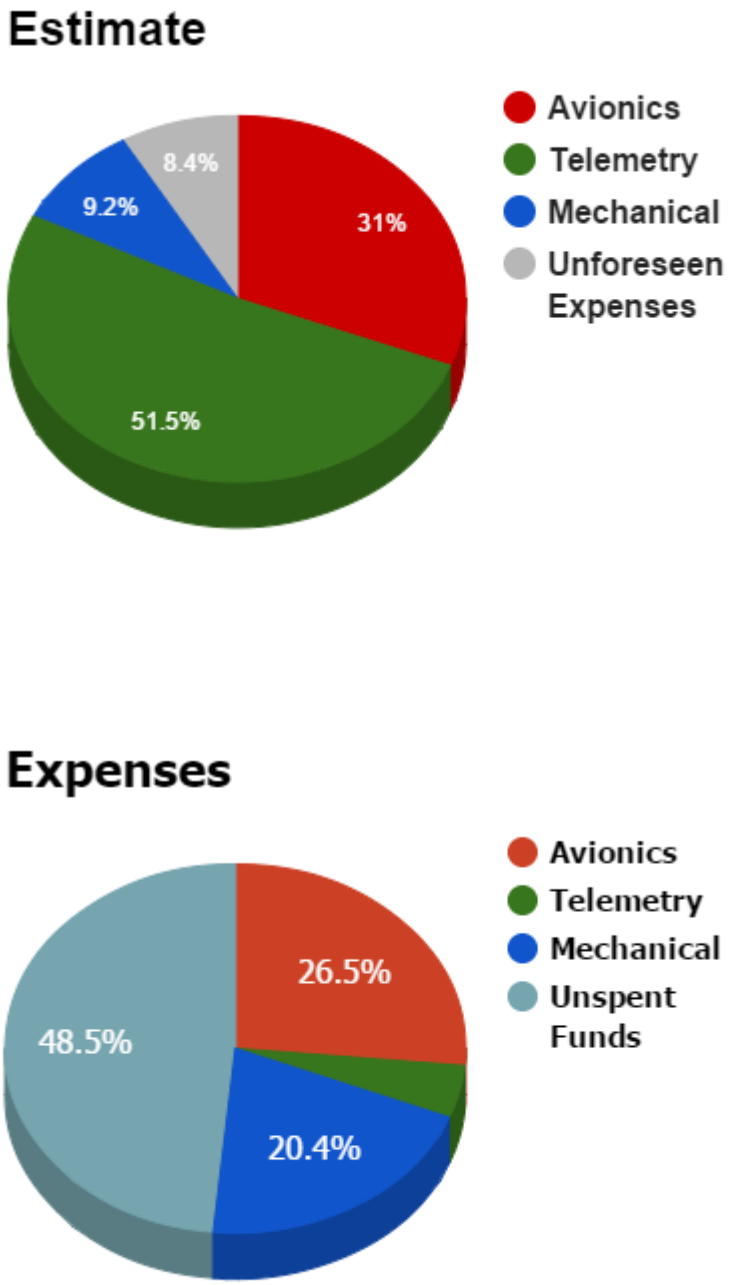

Figure C6. Comparison between the estimated and final budget for each subteam.